State-of-the-Art Harmonic-Balance Simulation of Forced Nonlinear Microwave Circuits by the Piecewise Technique

Vittorio Rizzoli, *Senior Member, IEEE,* Alessandro Lipparini, *Member, IEEE,* Alessandra Costanzo, Franco Mastri, Claudio Cecchetti, *Member, IEEE,* Andrea Neri, *Member, IEEE* and Diego Masotti

Abstract—**The paper discusses the theoretical foundations and the numerical performance of an advanced nonlinear circuit simulator based on the piecewise harmonic-balance (HB) technique. The program incorporates updated versions of several novel algorithmic concepts developed in the last few years. This results in computational capabilities well ahead of the state of the art of HB techniques as outlined even in recent review work. The exact computation of the Jacobian matrix for Newton-iteration based HB simulation, and the related conversion-matrix technique for fast mixer analysis, are formulated in the most general form available to date. Convergence problems at high drive levels are solved by a parametric formulation of the device models coupled with an advanced norm-reducing iteration. A physics-based approximation allows the HB equations to be effectively decoupled in many practical cases, thus bringing large-size jobs such as pulsed-RF analysis well within the reach of ordinary workstations. The exact Jacobian is used in conjunction with an exact formula for the gradient of the objective function, to implement an efficient broadband nonlinear circuit optimization capability. Finally, a number of examples are presented, in order to give the reader a feeling of the numerical performance that the program can provide at the workstation level.**

I. Introduction

IN THE last few years, the harmonic-balance (HB) method has gained widespread acceptance among microwave engineers as a simulation tool for nonlinear circuits. The main advantages of this approach are its ability to directly address the steady-state circuit operation under single- or multiple-tone excitation, and its full compatibility with the characterization of the linear subnetwork in the frequency domain, which is usually a prerequisite for high-frequency applications. Also, harmonic balance [1] and in the statistical design [2] of nonlinear microwave circuits.

In exchange for this, the HB method in its conventional implementations suffers from a number of shortcomings [3], which have traditionally restricted its domain of applicability to selected aspects of the general nonlinear CAD problem. By harmonic balance, a nonlinear circuit analysis is reduced to the solution of a nonlinear algebraic system, which is usually obtained by some sort of iterative procedure. In traditional HB simulators, as the exciting signal levels are increased, the system becomes more and more ill-conditioned, and the iteration slows down and eventually fails. Thus it is usually taken for granted that harmonic balance handles extremely nonlinear behavior poorly. A basic assumption of harmonic balance is always that the circuit be excited by one or more sinusoidal signals, so that all time-dependent quantities have a periodic or quasi-periodic steady-state dependence on time, and a same spectrum consisting of a finite set of intermodulation products of the exciting tones. Thus it is generally acknowledged that transient information cannot be produced by harmonic-balance analysis. The size of the solving system is equal to the number of state variables times the number of spectral lines. For multiple-device circuits excited by multiple tones, this may lead to nonlinear problems with thousands of unknowns, which may be impossible to deal with by conventional techniques. This fatally places an upper bound to the size of the circuit problems that can be solved by the HB technique, from the standpoint of both memory occupation and CPU time. One of the main challenges of harmonic-balance simulation is the extension of this bound.

This paper describes an advanced HB simulator incorporating new algorithmic concepts whereby the above-mentioned limitations of harmonic-balance analysis can be effectively overcome in many practical applications. The program makes use of the "piecewise" technique based on circuit decomposition [4]. This was preferred to the nodal HB approach [5] because it leads to a solving system much smaller in size [6], and allows the linear subnetwork description to be refined to any desired extent (e.g., by taking into account various kinds of disconti-

Manuscript received April 11, 1991. This work was partly sponsored by the Italian Ministry of University and Scientific Research and by the Istituto Superiore delle Poste e delle Telecomunicazioni (ISPT)

V. Rizzoli, A. Lipparini, and A. Costanzo are with the Dipartimento di Elettronica, Informatica e Sistemistica, University of Bologna, Villa Griffone, 40044 Pontecchio Marconi, Bologna, Italy.

F. Mastri is with the Instituto di Elettrotecnica, University of Bologna, Via Risorgimento 2, 40136 Bologna, Italy.

C. Cecchetti and A. Neri are with Fondazione Ugo Bordoni, Villa Griffone, 40044 Pontecchio Marconi, Bologna, Italy.

D. Masotti is with Fondazione Guglielmo Marconi, Villa Griffone, 40044 Pontecchio Marconi, Bologna, Italy.

IEEE Log Number 9103895.

nuities and couplings) without affecting the nonlinear analysis cost. Section II of the paper reviews an advanced formulation of the Newton-iteration based piecewise HB technique, making use of the exact Jacobian matrix in the general multitone analysis case. The same section also shows that the HB analysis automatically produces the fundamental information required for the noise and stability analysis of a nonlinear circuit. Section III demonstrates that virtually any limitation of the power-handling capabilities of harmonic-balance analysis can be eliminated by resorting to a parametric form of the nonlinear device equations coupled with an advanced norm-reducing mechanism. Section IV introduces a sparse-matrix approach explicitly tailored for the needs of the piecewise technique, allowing many large simulation tasks involving several thousands of unknowns to be brought well within the reach of ordinary engineering workstations. Section V discusses how the combination of the extended power-handling capabilities and of the sparse-matrix technique described in the preceding sections opens the way to the analysis of strongly nonlinear circuits under pulsed-RF conditions. This implies that transient information may be produced by harmonic-balance analysis in many cases of practical interest. Finally, Section VI shows that the Newton-iteration based HB analysis can be successfully coupled with an optimization algorithm, and that the numerical optimization of broadband nonlinear circuits becomes possible in this way, with an algorithmic efficiency comparable to that of linear circuit optimization.

With the above features, this program is believed to mark a significant advance over other previously reported harmonic-balance simulators, and to provide a suitable basis for the further extensions of nonlinear CAD capabilities which will be required for the years to come.

II. Newton-Iteration Based Harmonic-Balance Analysis

A. General Nonlinear Analysis

Let us consider a nonlinear microwave circuit operating in a quasi-periodic electrical regime generated by the intermodulation of F sinusoidal tones of incommensurable fundamental angular frequencies ω_i. Any signal $a(t)$ supported by the circuit may be represented by the multiple Fourier expansion

$$a(t) = \sum_{k \in S} A_k \exp(j\Omega_k t) \tag{1}$$

where Ω_k is a generic mixing or intermodulation (IM) product of the fundamentals, i.e.,

$$\Omega_k = \sum_{i=1}^{F} k_i \omega_i = \boldsymbol{k}^T \boldsymbol{\omega}_v. \tag{2}$$

In (1), (2) k_i is an integer harmonic number, $\boldsymbol{k}$ is an F-vector of harmonic numbers, and $\boldsymbol{\omega}_v$ is the F-vector of the fundamentals. The vector $\boldsymbol{k}$ in (2) spans a finite subset $\boldsymbol{S}$ of the $\boldsymbol{k}$-space (containing the origin) which will be conventionally named the *signal spectrum*. The Fourier coefficient A_k will be named the *harmonic* of $a(t)$ at Ω_k (or the kth harmonic of $a(t)$). The order of Ω_k is defined as the ℓ_1 norm of $\boldsymbol{k}$. Since we want the signal (1) to be real, $\boldsymbol{S}$ must be symmetrical with respect to the origin, and $A_{-k} = A_k^*$. We shall also denote by $\boldsymbol{S}^+$ the subset of $\boldsymbol{S}$ such that $\Omega_k \geq 0$ for $\boldsymbol{k} \in \boldsymbol{S}^+$.

Let the nonlinear subnetwork be described by the generalized parametric equations [6]

$$\begin{aligned} \boldsymbol{v}(t) &= \boldsymbol{u}\left[\boldsymbol{x}(t), \frac{d\boldsymbol{x}}{dt}, \cdots, \frac{d^n\boldsymbol{x}}{dt^n}, \boldsymbol{x}_D(t)\right] \\ \boldsymbol{i}(t) &= \boldsymbol{w}\left[\boldsymbol{x}(t), \frac{d\boldsymbol{x}}{dt}, \cdots, \frac{d^n\boldsymbol{x}}{dt^n}, \boldsymbol{x}_D(t)\right] \end{aligned} \tag{3}$$

where $\boldsymbol{v}(t)$, $\boldsymbol{i}(t)$ are vectors of voltages and currents at the common ports, $\boldsymbol{x}(t)$ is a vector of state variables and $\boldsymbol{x}_D(t)$ a vector of time-delayed state variables, i.e., $x_{D_i}(t) = x_i(t - \tau_i)$. The time delays τ_i may be functions of the state variables [7]. All vectors in (3) have a same size n_d equal to the number of common (device) ports. This kind of representation is very convenient from the physical viewpoint, because it is in fact equivalent to a set of implicit integro-differential equations in the port currents and voltages. This allows an effective minimization of the number of subnetwork ports [6], and, what is more important, results in extreme generality in device modeling capabilities. A major practical implication of this approach will be demonstrated in Section III.

The quasi-periodic electrical regime of the nonlinear circuit resulting from a multitone excitation is completely defined by a set of time-dependent state variables of the form (1), or equivalently by the vector $\boldsymbol{X}$ of the real and imaginary parts of their harmonics. The size of this vector is $N_T = n_d n_H$, where n_H is the cardinality of the spectrum $\boldsymbol{S}$. The entries of $\boldsymbol{X}$ represent the problem unknowns. In order to compute the harmonics $\boldsymbol{U}_k$, $\boldsymbol{W}_k$ of the nonlinear subnetwork response (3) to the multitone excitation described by a vector $\boldsymbol{X}$, the program makes use of the multiple fast Fourier transform (MFFT). The general-purpose application of this algorithm to nonlinear microwave circuit analysis was first reported in [8], and a detailed description of its implementation in a CAD environment is given in [6]. The excellent performance of the MFFT has been recently acknowledged by several authors (e.g., [9], [10]).

The linear subnetwork may be represented by the frequency-domain equation

$$\boldsymbol{Y}(\omega)\, \boldsymbol{V}(\omega) + \boldsymbol{N}(\omega) + \boldsymbol{I}(\omega) = 0 \tag{4}$$

where $\boldsymbol{V}(\omega)$, $\boldsymbol{I}(\omega)$ are vectors of voltage and current phasors, $\boldsymbol{Y}(\omega)$ is the linear subnetwork admittance matrix, and $\boldsymbol{N}(\omega)$ is a vector of Norton equivalent current sources. Thus the set of complex harmonic-balance errors at a generic IM product Ω_k has the expression

$$\boldsymbol{E}_k(\boldsymbol{X}) = \boldsymbol{Y}(\Omega_k)\, \boldsymbol{U}_k(\boldsymbol{X}) + \boldsymbol{N}(\Omega_k) + \boldsymbol{W}_k(\boldsymbol{X}) \tag{5}$$

The nonlinear analysis problem is reduced to the solution of a nonlinear algebraic system by imposing that all the HB errors vanish. In order to avoid the use of negative frequencies, the nonlinear solving system is formulated in terms of a vector $\boldsymbol{E}$ of real and imaginary parts of the HB errors given by (5) for $\boldsymbol{k} \in \boldsymbol{S}^+$, and is thus written as a system of N_T real equations in N_T unknowns, namely

$$\boldsymbol{E}(\boldsymbol{X}) = \boldsymbol{0} \tag{6}$$

Although many iterative schemes are available for solving (6), the Newton–Raphson method has been preferred for a number of reasons that will become apparent from the following discussion. More precisely, we use a norm-reducing Newton iteration defined by [11]

$$\boldsymbol{X}^{(n+1)} = \boldsymbol{X}^{(n)} - \alpha_n \{\boldsymbol{J}[\boldsymbol{X}^{(n)}]\}^{-1} \boldsymbol{E}[\boldsymbol{X}^{(n)}] \tag{7}$$

where $\boldsymbol{X}^{(n)}$ is the nth iterate in the unknown $\boldsymbol{X}$, and α_n is a scalar damping parameter. For later convenience (see Section IV) the Jacobian matrix of $\boldsymbol{E}$ with respect to $\boldsymbol{X}$ (namely, $\boldsymbol{J}(\boldsymbol{X})$ in (7)) is partitioned frequency-wise into $2n_d \times 2n_d$ submatrices of the form ($\boldsymbol{k}, \boldsymbol{s} \in \boldsymbol{S}^+$)

$$\boldsymbol{J}_{k,s} = \begin{bmatrix} \dfrac{\partial \operatorname{Re}[\boldsymbol{E}_k]}{\partial \operatorname{Re}[\boldsymbol{X}_s]} & \dfrac{\partial \operatorname{Re}[\boldsymbol{E}_k]}{\partial \operatorname{Im}[\boldsymbol{X}_s]} \\ \dfrac{\partial \operatorname{Im}[\boldsymbol{E}_k]}{\partial \operatorname{Re}[\boldsymbol{X}_s]} & \dfrac{\partial \operatorname{Im}[\boldsymbol{E}_k]}{\partial \operatorname{Im}[\boldsymbol{X}_s]} \end{bmatrix}. \tag{8}$$

To ensure the best performance of the Newton algorithm it is of paramount importance that the Jacobian matrix of the HB errors with respect to the unknowns be computed by an exact algorithm, rather than by numerical perturbations. This has the twofold advantage of being faster and much more accurate. The derivatives evaluated by perturbations rapidly degrade as the number of nonlinear devices and/or harmonics is increased. The required number of iterations is in some way inversely related to the accuracy of the Jacobian, so that beyond some threshold, convergence begins to slow down and eventually fails at all. As an example, let us consider the distributed DGFET mixer schematically illustrated in Fig. 1 [12]. At typical drive levels, the analysis time for this kind of circuit decreases by a factor of more than 100 when the perturbational derivatives are replaced by the exact ones.

The algorithm for the computation of the exact derivatives is detailed below. General formulae for the piecewise analysis under multitone excitation were first presented in [6], and are further extended here to cover the case of state-dependent time delays. From (5) we get

$$\frac{\partial \boldsymbol{E}_k}{\partial \operatorname{Re}[\boldsymbol{X}_s]} = \boldsymbol{Y}(\Omega_k) \frac{\partial \boldsymbol{U}_k}{\partial \operatorname{Re}[\boldsymbol{X}_s]} + \frac{\partial \boldsymbol{W}_k}{\partial \operatorname{Re}[\boldsymbol{X}_s]}$$

$$\frac{\partial \boldsymbol{E}_k}{\partial \operatorname{Im}[\boldsymbol{X}_s]} = \boldsymbol{Y}(\Omega_k) \frac{\partial \boldsymbol{U}_k}{\partial \operatorname{Im}[\boldsymbol{X}_s]} + \frac{\partial \boldsymbol{W}_k}{\partial \operatorname{Im}[\boldsymbol{X}_s]} \tag{9}$$

for all $\boldsymbol{k}, \boldsymbol{s} \in \boldsymbol{S}^+$. The derivatives of the voltage and current harmonics $\boldsymbol{U}_k$, $\boldsymbol{W}_k$ are found in the following way.

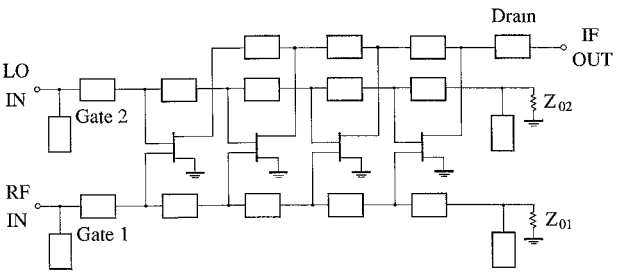

Fig. 1. Schematic topology of a distributed 4-stage DGFET mixer.

For the voltages (e.g.) we first introduce the Fourier expansions

$$\frac{\partial \boldsymbol{u}}{\partial \boldsymbol{y}_m} = \sum_{p \in S_d} \boldsymbol{C}_{m,p} \exp(j\Omega_p t)$$

$$\frac{\partial \boldsymbol{u}}{\partial \boldsymbol{x}_D} = \sum_{p \in S_d} \boldsymbol{C}_p^D \exp(j\Omega_p t) \tag{10}$$

where $\boldsymbol{y}_0 = \boldsymbol{x}$, $\boldsymbol{y}_m = d^m\boldsymbol{x}/dt^m$ ($1 \le m \le n$), and $\boldsymbol{S}_d$ will be named the *derivatives spectrum*. When the nonlinear device equations (3) are very complicated (or even numerically defined), the time-domain derivatives on the left-hand side of (10) may be computed numerically, though the best performance of the algorithm is obtained when exact closed-form expressions can be found for these quantities.

The derivatives of the voltage harmonics with respect to the state variable harmonics can now be obtained from the first of (3) for $\boldsymbol{k}, \boldsymbol{s} \in \boldsymbol{S}^+$:

$$\frac{\partial \boldsymbol{U}_k}{\partial \operatorname{Re}[\boldsymbol{X}_s]} = \sum_{m=0}^{n} (j\Omega_s)^m [\Gamma_{m,k-s} + (-1)^m \Gamma_{m,k+s}]$$

$$\frac{\partial \boldsymbol{U}_k}{\partial \operatorname{Im}[\boldsymbol{X}_s]} = \sum_{m=0}^{n} j(j\Omega_s)^m [\Gamma_{m,k-s} - (-1)^m \Gamma_{m,k+s}] \tag{11}$$

where

$$\Gamma_{m,k-s} = \boldsymbol{C}_{m,k-s} + \delta_m^0 \sum_{p \in S} \boldsymbol{C}_{k-p}^D \frac{\partial \boldsymbol{X}_p^D}{\partial \boldsymbol{X}_s}$$

$$\Gamma_{m,k+s} = \boldsymbol{C}_{m,k+s} + \delta_m^0 \sum_{p \in S} \boldsymbol{C}_{k-p}^D \frac{\partial \boldsymbol{X}_p^D}{\partial \boldsymbol{X}_{-s}}$$

$$(0 \le m \le n). \tag{12}$$

and $\boldsymbol{X}_p^D$ is the set of pth harmonics of $\boldsymbol{x}_D(t)$ (δ = Kronecker's symbol). Although an exact expression has been obtained for $\partial \boldsymbol{X}_p^D / \partial \boldsymbol{X}_s$, it is so complicated that a numerical computation of this quantity is usually preferred. In the case of constant delays, this derivative reduces to $\delta_p^s \exp(-j\Omega_s\tau)$ where τ is the diagonal matrix of the time delays [6]. Note that when $\boldsymbol{k}$, $\boldsymbol{s}$ span the set $\boldsymbol{S}^+$, their combinations $\boldsymbol{k} \pm \boldsymbol{s}$ span a larger set of the $\boldsymbol{k}$ space, so that the derivatives spectrum $\boldsymbol{S}_d$ must usually be larger than $\boldsymbol{S}$ in order to make available all the necessary infor-

mation. Similar expressions hold for the derivatives of the current harmonics.

The Newton-iteration based HB technique making use of exact derivatives is very efficient from the numerical viewpoint. As an example, let us assume that the mixer in Fig. 1 is excited by a +13 dBm local oscillator (corresponding to a maximum of the conversion gain) at 3 GHz, and by a −20 dBm RF signal at 3.51 GHz. 4 LO harmonics and the associated sidebands are retained in the simulation, for a total of 13 frequencies plus dc. Taking into account only the essential parasitic effects results in a circuit topology with 16 device ports and 57 circuit nodes. In such conditions, the analysis requires about 75 CPU's on a SUN SPARCstation 2 starting from zero harmonics, and treating the Jacobian matrix as dense. A further speedup can be obtained making use of the sparse-matrix technique discussed in Section IV. Also, thanks to the use of continuation, the algorithm becomes really fast on a power sweep. As an example, if in the same mixer analysis the RF power is swept from −20 to +3 dBm with 1 dB steps (the upper bound corresponds to a gain compression of about 1.2 dB), the average analysis cost drops to about 10 s per point.

B. Frequency-Conversion Analysis

It has become customary to define *frequency-conversion analysis* a linearized form of multitone intermodulation analysis which becomes possible when a small independent signal is fed into a nonlinear circuit operated in a large-signal periodic or quasi-periodic steady-state regime. This is a very classic problem that has received a number of treatments, and has been primarily applied in the microwave field to mixer analysis under the assumption of a small RF signal superimposed on a large LO drive.

The basic mathematical tool for a frequency-conversion analysis is given by the conversion equations of the nonlinear subnetwork. Let us assume that a steady-state of the form (1) is perturbed by the injection of a sinusoidal signal of angular frequency ω. If the perturbation is small enough, it can be studied by linearizing the nonlinear subnetwork equations in the neighborhood of the unperturbed steady state. This implies that the perturbed steady state may be represented as a quasi-periodic regime containing only intermodulation products of first order with respect to the perturbation. A generic signal supported by the circuit thus takes the form

$$a(t) = a_{ss}(t) + \sum_{k \in S} \Delta A_k \exp\left[j(\omega + \Omega_k)t\right] \quad (13)$$

where $a_{ss}(t)$ is the unperturbed steady state given by (1). Note that the signal on the right-hand side of (13) is complex, but this has no influence on the analysis since we are only interested in the relationships among the sideband phasors.

Due to the linearization, the phasors of the voltage and current harmonics at the sidebands are linearly related by the so-called *conversion equations* of the nonlinear subnetwork. If the nonlinear devices are described by the parametric equations (3), the conversion equations are also expressed in parametric form as follows [13]

$$\Delta \boldsymbol{V} = \boldsymbol{P}\,\Delta \boldsymbol{X}$$
$$\Delta \boldsymbol{I} = \boldsymbol{Q}\,\Delta \boldsymbol{X} \quad (14)$$

Specifically, these equations are linear maps between the spectra of the perturbations on voltages ($\Delta \boldsymbol{V}$), currents ($\Delta \boldsymbol{I}$), and state variables ($\Delta \boldsymbol{X}$). The corresponding linear operators $\boldsymbol{P}$, $\boldsymbol{Q}$ are called *conversion matrices*. From (14) any equivalent circuit description such as the impedance, admittance, or scattering conversion matrix can be derived by conventional circuit algebra.

The conversion matrices may be computed by replacing the perturbed expressions (13) of the state variables into (3) and making use of (10). If we partition $\boldsymbol{P}$ and $\boldsymbol{Q}$ frequency-wise into complex submatrices of size $n_d \times n_d$ ($\boldsymbol{k}$, $s \in \boldsymbol{S}$), we obtain the final result

$$\boldsymbol{P}_{k,s} = \sum_{m=0}^{n} \left\{ [j(\omega + \Omega_s)]^m \boldsymbol{C}_{m,k-s} + \delta_m^0 \sum_{p \in S} \boldsymbol{C}^D_{k-p} \boldsymbol{B}_{p-s}(\omega + \Omega_s) \right\}$$
$$\boldsymbol{Q}_{k,s} = \sum_{m=0}^{n} \left\{ [j(\omega + \Omega_s)]^m \boldsymbol{D}_{m,k-s} + \delta_m^0 \sum_{p \in S} \boldsymbol{D}^D_{k-p} \boldsymbol{B}_{p-s}(\omega + \Omega_s) \right\} \quad (15)$$

where the $\boldsymbol{D}$ matrices are coefficients of Fourier expansions similar to (10) for the derivatives of the second of (3). The $n_d \times n_d$ diagonal matrices $\boldsymbol{B}$ appearing in (15) are the coefficients of the Fourier expansions

$$\exp\left\{-j(\omega + \Omega_s)\tau[\boldsymbol{x}_{ss}(t)]\right\} = \sum_{p \in S_d} \boldsymbol{B}_p(\omega + \Omega_s) \exp\left(j\Omega_p t\right). \quad (16)$$

In the case of constant time delays, $\boldsymbol{B}_p(\omega + \Omega_s)$ reduces to $\delta_p^0 \exp\left[-j(\omega + \Omega_s)\tau\right]$.

A comparison between (15) and (9), (11) makes evident the close relationship existing between the conversion matrix and the Jacobian matrix. The key point is that the essential information required to generate the conversion matrices (specifically, the coefficients $\boldsymbol{C}$, $\boldsymbol{D}$) is the same needed for the computation of the Jacobian (the additional Fourier transformations (16) are only required in the case of state-dependent time delays). As it is well known, the conversion matrices provide the computational basis for a generalized noise and stability analysis of the nonlinear circuit [13]. It is thus clear that the Newton-iteration based harmonic-balance technique appears to be the best candidate for the development of a general-purpose nonlinear CAD system integrating several advanced simulation capabilities in a most efficient way. We shall see in Section VI that the same conclusion can also be extended to nonlinear circuit optimization.

The frequency-conversion approach is usually computationally convenient with respect to the full nonlinear analysis for the simulation of microwave mixers at low RF power levels, especially for complex multiple-device topologies. As an example, the analysis of the mixer in Fig. 1 with an LO power of +13 dBm takes about 12 s on a SUN SPARCstation 2. The results are virtually identical to those obtained from the full nonlinear analysis with −20 dBm RF power. Of course, the dynamic range of the mixer cannot be determined by this method.

III. Enhancing the Power-Handling Capabilities

The iteration (7) (as well as any other iterative scheme) may exhibit convergence problems at high drive levels, in a way strongly dependent on the particular problem being considered. Specifically, some of the most important factors affecting the speed of convergence or the ability to converge at all, are the degree of device nonlinearity, the number of intermodulating tones, and topological aspects such as the number of nonlinear devices and the way they are interconnected. For instance, the exponential behavior of the conduction current of p-n and Schottky barriers is usually a major source of numerical ill-conditioning [14], and so is the unidirectional nature of the nonlinear transconductance of microwave active devices [11].

The exact computation of the Jacobian matrix described in the previous section usually gives an important contribution to the robustness of the analysis algorithm, but is not sufficient to cover all cases of practical interest. In order to improve the power-handling capabilities, many harmonic-balance simulators make use of source stepping, which can be considered a CAD implementation of the mathematical concept of continuation, or homotopy [15]. Source stepping is computationally inefficient, though, unless a specific interest exists in the results of a power sweep, since it expands a single analysis into a sequence of HB simulations. What is more important, this technique is far from providing a general solution to the problem, since in many ill-conditioned cases the step size required to achieve convergence is too small, and the analysis becomes exceedingly slow. As a limiting case, the algorithm fails to converge if the step size drops below the computer precision. In this section we describe a totally different approach, based on a special parametric description of the device nonlinearities coupled with an advanced norm-reducing iteration scheme [16]. It will be shown that this method virtually eliminates any limitation of the power-handling capabilities of HB analysis, with no need for source stepping.

In order to illustrate the modeling approach we consider the exponential junction law, which is by far one of the most critical issues [14]. The conventional p-n or Schottky-barrier current equation is

$$i(t) = I_S\{\exp[\alpha v(t)] - 1\} \tag{17}$$

At high drive levels the exponential function appearing in (17) is a strong source of numerical ill-conditioning. To replace (17) by a well-conditioned junction model for $v > 0$, we resort to a parametric representation of the form (3) making use of a non-conventional choice of the state variable. Instead of the junction voltage $v(t)$, we take as the state variable a fictitious quantity $x(t)$ which is identical to the junction voltage below some threshold $V_1 > 0$, but is defined as a linear function of the current above V_1. By requiring the voltage and current and their derivatives to be continuous at $x = V_1$, we obtain the following set of equations:

$$v(t) = u[x(t)] = \begin{cases} V_1 + \dfrac{1}{\alpha}\ln\{1 + \alpha[x(t) - V_1]\} \\ \qquad \text{if } V_1 \le x(t) \\ x(t) \qquad \text{if } x(t) \le V_1 \end{cases} \tag{18}$$

$$i(t) = w[x(t)] = \begin{cases} I_S \exp(\alpha V_1)\{1 + \alpha[x(t) - V_1]\} - I_S \\ \qquad \text{if } V_1 \le x(t) \\ I_S\{\exp[\alpha x(t)] - 1\} \qquad \text{if } x(t) \le V_1. \end{cases} \tag{19}$$

Equations (18) and (19) give an exact parametric representation of the forward current-voltage characteristic (17) by means of functions which are very well conditioned for all values of $x(t)$. V_1 plays the role of a free parameter to be suitably chosen in order to optimize the performance of the HB algorithm. If we introduce the slope $G_1 = di/dv$ at $v = V_1$, we obtain from (17) $V_1 = ln\,(G_1/\alpha I_S)/\alpha$. Experience shows that the choice $G_1 = 1$ results in excellent numerical behavior of the model in most practical situations.

In order to show the beneficial effects of the above method on the convergence properties of the Newton iteration, we resume a very famous convergence test consisting of the local-oscillator analysis for a simple waveguide mixer containing a resistive diode as the only nonlinear component. This test was first considered by Kerr [17] and subsequently used for comparison by Hicks and Khan [18], Camacho-Peñalosa [19], and Schüppert [20]. The ability to converge is measured in terms of the number of iterations required to achieve a minimum relative accuracy of 10^{-3} on all the spectral components, and the rectified dc component of the diode current is taken as an indication of the drive level. The analysis uses 16 local oscillator harmonics and the iteration is started from zero harmonics in all cases.

Fig. 2 shows a performance comparison among a number of iterative approaches to the solution of the system (6), that is: 1), Hicks and Khan's constant-p fixed-point iteration [18]; 2), Camacho-Peñalosa's fixed-point iteration with automatically updated convergence parameters [19]; 3), Schüppert's iteration making use of convergence parameters related to the diode effective harmonic impedances [20]; 4), an undamped Newton iteration ($\alpha_n = 1$ in

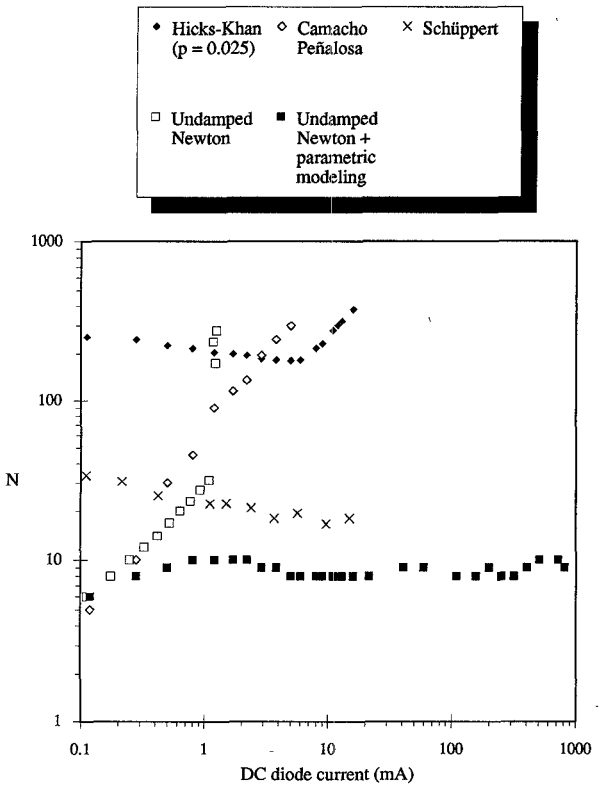

Fig. 2. Performance comparison of several harmonic-balance algorithms in the solution of Kerr's waveguide diode mixer.

(7)) based on the conventional model (17); 5), an undamped Newton iteration based on the parametric model (18), (19). Typically, for each iteration scheme there exists a critical power level beyond which convergence slows down or is lost at all. In particular, the convergence properties of the conventional Newton iteration are definitely poor: the iteration fails to converge above a dc current of the order of 1.5 mA, corresponding to a drive level of only 15 mW. Note, however, that the use of the parametric model results in a dramatic increase of the power-handling capabilities of the analysis algorithm. In this case the input power range for which convergence is achieved is found to be substantially unbound, and the number of required iterations remains fairly constant up to very high power levels, with no need for source stepping. The range shown in Fig. 2 goes up to a current level of 1 A, corresponding to an input power of more than 1 kW, but this does not represent an upper bound.

Generally speaking, this approach can be extended to all major sources of ill-conditioning in the most commonly used nonlinear device models, including forward conduction and breakdown effects in diodes and FET's, diffusion capacitances in p-n diodes and bipolar transistors [16], [21], and so on. So this really represents the seed of a generalized modeling philosophy marking a big step towards the elimination of large-signal problems in harmonic-balance analysis.

The other key mechanism of convergence improvement that has been implemented in the program is norm reduction. Given the basic iterative solution scheme (7), we have a norm-reducing iteration when the damping parameter is updated at each step in such a way that the norm of the residual error vector decreases with respect to the previous step, i.e.,

$$\|\boldsymbol{E}[\boldsymbol{X}^{(n+1)}]\| < \|\boldsymbol{E}[\boldsymbol{X}^{(n)}]\| \tag{20}$$

The norm may be generally defined as

$$\|\boldsymbol{E}[\boldsymbol{X}^{(n)}]\| = \sqrt{\boldsymbol{E}^T[\boldsymbol{X}^{(n)}]\,\boldsymbol{A}_n\boldsymbol{E}[\boldsymbol{X}^{(n)}]} \tag{21}$$

where $\boldsymbol{A}_n$ is an arbitrary positive-definite matrix. In practice, in order to get as much as possible from this basic idea, the coefficient α_n in (7) is chosen in such a way as to minimize the norm along the direction of the iteration update, at least approximately by a coarse one-dimensional search.

The commonly adopted definition of norm is the Euclidean or ℓ_2 norm which is obtained from (21) when $\boldsymbol{A}_n$ is an identity matrix. With this choice, norm reduction can be used in conjunction with virtually any iteration scheme. As an example, Haywood and Chow [22] used norm reduction to improve the performance of Hicks and Khan's fixed-point iteration [18]. With the Newton iteration, superior performance may be obtained making use of the *Newton-Update* (NU) norm introduced by Yeager and Dutton [11], which is defined by

$$\boldsymbol{A}_n = \{\boldsymbol{J}^T[\boldsymbol{X}^{(n)}]\}^{-1}\{\boldsymbol{J}[\boldsymbol{X}^{(n)}]\}^{-1}. \tag{22}$$

For computational purposes the NU norm is replaced by the Euclidean norm of the undamped Newton update computed at the new point with the Jacobian of the previous step [11], i.e.,

$$\|\boldsymbol{E}[\boldsymbol{X}^{(n+1)}]\|_{NU} = \|\{\boldsymbol{J}[\boldsymbol{X}^{(n)}]\}^{-1}\boldsymbol{E}[\boldsymbol{X}^{(n+1)}]\|_{\ell_2}. \tag{23}$$

The NU norm was used in [11] in the time-domain simulation of nonlinear circuits, and has been found by the present authors to be equally effective in harmonic-balance applications [16]. The damping mechanism based on the Euclidean norm emphasizes a uniform or unweighted reduction of the residual errors. This has been observed [11] to be very dangerous for those situations where the Jacobian matrix has large nonsymmetric off-diagonal terms, since the steepest-descent direction of the norm tends to become nearly orthogonal to the direction of the Newton update. If this happens, typically in the early steps of the iteration, no amount of damping can significantly reduce the norm, the damping parameter tends to zero and the iteration fails. Unfortunately, this situation is rather commonplace in microwave circuit analysis by the harmonic-balance method, since it is typical of nonreciprocal gain elements such as FET's or bipolar transistors, especially when cascaded in multistage topologies. With the NU norm the residual errors are weighted by the elements of the inverse Jacobian before computing the Euclidean norm. The magnitude of a generic element of the resulting vector indicates how far the corresponding unknown is from achieving convergence, and may thus be interpreted as a measure of the relative priority of such unknown in

the overall solution process. The damping strategy thus emphasizes a uniform reduction of such priorities through a weighted reduction of the residual errors. The superior performance of this approach is due to the fact that the steepest-descent direction for the NU norm is always coincident with the direction of the Newton update [11]. Thus even in the above-mentioned ill-conditioned cases the danger of convergence failure in the early steps of the iteration is most often eliminated. The damping factor usually oscillates but does not approach zero along the iteration.

In order to illustrate the impact of these techniques on the power-handling capabilities of harmonic-balance analysis, we report on a three-tone intermodulation test for the distributed amplifier depicted in Fig. 3. This is a simple small-signal device optimized for a 5 dB gain across the 2–18 GHz band, with an output power of +20 dBm at the 1 dB compression point. The numerical results are given in Fig. 4. The ability of the analysis algorithm to converge is measured in terms of the number of iterations required to achieve a relative accuracy of 10^{-5} on all the intermodulation products of the three fundamentals, up to the 4th order. This number is plotted in Fig. 4 against the available input power per tone P_{in}. The comparison is among four different implementations of the Newton method, with and without parametric modeling and NU-norm reduction; in all cases, the analysis is always started from zero harmonics without source stepping.

As usual, the plain Newton iteration using the conventional models has poor behavior, and only converges in the linear region, up to approximately $P_{in} = +10$ dBm. This bound is expanded to $P_{in} = +24$ dBm by using parametric modeling without norm reduction, and to $P_{in} = +50$ dBm with norm reduction and conventional models. Note that in this special case the convergence improvement provided by parametric modeling is not as important as that obtained by norm reduction. However, in the region where both methods are successful, the former is definitely faster since it does not require the iterative search for the optimum α_n in (7). Finally, coupling norm reduction with parametric modeling leads to an extremely robust analysis algorithm, which in the present case can handle up to +100 dBm (10 MW) per tone, with a fairly constant number of iterations. An interesting point is that we need not increase the number of harmonics to achieve convergence even at extremely high power levels, though of course the accuracy of the solution will generally depend on this number. Similar results have been obtained for multistage cascaded topologies [16] and even for class-C bipolar transistor amplifiers [23].

It is now clear that the techniques described in this section can broadly overcome those power-handling limitations that have long been considered an important disadvantage of harmonic balance in comparison with other competing nonlinear analysis algorithms such as time-domain techniques. Although in practice we usually do not have to handle the extreme power levels that are referred to in Fig. 4, the availability of an absolutely reliable HB analysis mechanism may be of paramount importance for a successful performance of many nonlinear design tasks. As an example, for an efficient optimization of broadband

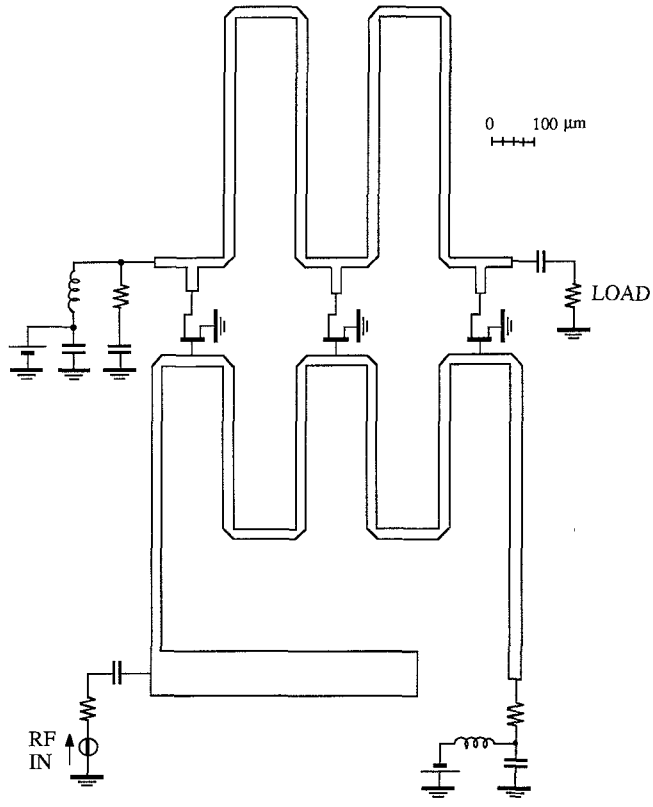

Fig. 3. Schematic topology of a distributed 3-stage FET amplifier.

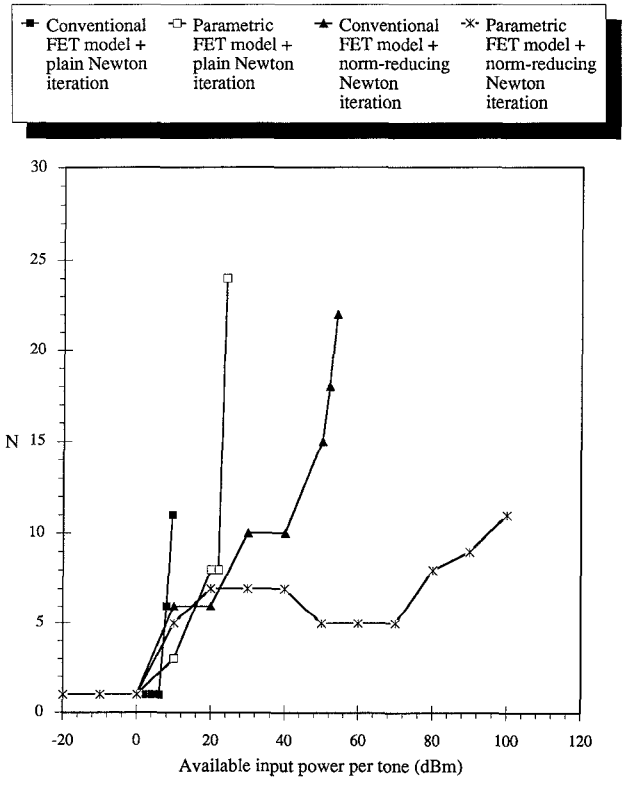

Fig. 4. Results of a 3-tone intermodulation analysis of the distributed amplifier.

power circuits it is essential that the analysis algorithm does never fail, even for circuit configurations that may be very ill-conditioned and hardly meaningful, but many nevertheless be encountered during the iterative search. Also, in such cases one usually does not want to use source stepping nor to increase the number of harmonics beyond the minimum dictated by accuracy requirements, in order to limit the computational effort. Thus the above-described techniques can significantly broaden the domain of practical application of nonlinear CAD methods.

IV. Sparse-Matrix Approach to Large-Size Problems

The considerable advantages of the Newton iteration making use of the exact Jacobian matrix as a numerical approach to the solution of the harmonic-balance system (6), have been demonstrated in the preceding sections. However, the straightforward application of this technique may become problematic when the number of scalar unknowns of the solving system becomes large, as it may be the case for multiple-device circuits under multitone excitation. This is due to the fact that the storage and factorization of the Jacobian by ordinary means are practically impossible when the number of unknowns exceeds some upper bound depending on the computer system in use. As a typical example, let us consider the analysis of two-tone intermodulation distortion in a mixer of the kind shown in Fig. 1. Following Maas [24], the signal spectrum for this analysis is defined by

$$\boldsymbol{S} \triangleq \begin{cases} 0 \le |k_1 + k_2 + k_3| \le N_O \\ 0 \le |k_2| + |k_3| \le M \end{cases} \tag{24}$$

where the subscript 1 is used for the local oscillator. In (24) N_O is the number of LO harmonics, and M is the maximum order of IM products of the two RF input tones that are taken into account. For $N_O = 4$, $M = 3$ the signal spectrum contains 225 lines, and the analysis requires 3600 unknowns ($n_d = 16$). In this case, the storage of the full Jacobian would require about 104 MB of memory, and one factorization would take many hours of CPU time on a typical workstation. Another class of problems resulting in very large-size numerical jobs will be discussed in the next section.

An obvious way to overcome these difficulties would be to resort to large computer systems such as vector processors [25]. However, in many practical applications where extreme power levels are not of concern, the exploitation of sparse-matrix techniques makes it possible to achieve a good compromise among power-handling capabilities, speed of convergence and memory occupation. The key idea is to set to zero selected entries of the Jacobian matrix according to some physical or mathematical criterion, in order to enhance its sparsity and thus to reduce memory occupation and factorization time. In general, computing the Jacobian with the highest possible accuracy maximizes the robustness and minimizes the number of iterations required for convergence of the Newton algorithm. However, in large-size problems where the factorization of the Jacobian represents a major contribution to the overall analysis cost, the use of an artificially sparse Jacobian may be computationally convenient, due to the tradeoff between number of iterations and cost of each one.

The actual implementation of these ideas may change considerably depending on the circuit analysis strategy. With the nodal approach, the circuit is analyzed as a whole without partitioning, and the node voltages are chosen as state variables [5]. The number of scalar unknowns is thus much larger than with the piecewise technique: for instance, the above-mentioned mixer IM analysis requires 12825 unknowns even if only the essential parasitic effects are accounted for (57 circuit nodes). In exchange for this, the Jacobian matrix is naturally sparse because so is the nodal admittance matrix, so that this method can routinely rely upon sparse-matrix techniques. A sparsity increase can thus be obtained by neglecting those entries that are smaller in magnitude than a specified threshold. This has the immediate advantage of enhancing the efficiency of the sparse-system solver [5].

With the piecewise method based on circuit decomposition, the situation is somewhat more complicated, since in this case the starting point is a completely dense Jacobian. This implies that the achievable sparsity, which may be typically of the order of 5 to 10% for medium-size jobs, is not sufficient for satisfactory operation of standard sparse-system solvers. A possible way of overcoming this difficulty is to create a sparsity pattern with the two properties of having a very simple structure and being *a priori* known [26], [27]. The basic idea for the method implemented in our program is suggested by the expressions (11) of the exact derivatives. As it was mentioned in Section II, the derivatives spectrum $\boldsymbol{S}_d$ used in the expansions (10) is generally different from the signal spectrum $\boldsymbol{S}$. At very high drive levels all the coefficients appearing in (11) must be taken into account to ensure good convergence, so that $\boldsymbol{S}_d \supset \boldsymbol{S}$. At lower drive levels, a good tradeoff between power-handling capabilities and analysis cost can usually be obtained by artificially reducing $\boldsymbol{S}_d$ and setting to zero in (11) all the coefficients for which $\boldsymbol{k} \pm \boldsymbol{s} \notin \boldsymbol{S}_d$. When the Jacobian is organized in submatrices frequency-wise in the way described in Section II, what one gets is a pattern of zero and nonzero submatrices of the form (8). Each submatrix is essentially dense because so is the admittance matrix of the linear subnetwork.

Generally speaking, this technique is very powerful for several reasons. Since the sparsity pattern is known *a priori*, one can avoid the use of general-purpose sparse-matrix solvers, and implement instead a family of specialized solvers, each individually optimized for a specific matrix structure, and making use of specific rules for addressing the nonzeros. This leads to an effective optimization of both memory storage and CPU time, and thus to an efficient performance of the sparse-system solvers even with very moderate degrees of sparsity, say of the order of 10%. Also, the sparse Jacobian can often be re-

duced to very simple structures for which the generation of fill-ins is a minimum or none at all. Finally, the structure of the sparse-matrix solver depends on the spectra $\boldsymbol{S}$, $\boldsymbol{S}_d$, but is topology-independent, i.e., the same solver can be applied to the analysis (with given spectra) of any nonlinear circuit, irrespective of its physical configuration.

A very important family of derivatives spectra is defined by the following equations:

$$\boldsymbol{S}_d \triangleq \begin{cases} 0 \le \sum_{i=1}^{H} |k_i| \le D \\ k_i = 0 \quad (H+1 \le i \le F) \end{cases} \tag{25}$$

where D, H are integers and $H < F$. Due to (11), under the second of (25) the mixing products Ω_k, Ω_s are considered uncoupled unless $|k_i| = |s_i|$ for $H + 1 \le i \le F$, because otherwise $\boldsymbol{k} \pm \boldsymbol{s} \notin \boldsymbol{S}_d$. Now let the signal spectrum be partitioned into H-dimensional subsets such that the mixing products belonging to each subset have the same $|k_i|$ for $H + 1 \le i \le F$. Since under the second of (25) any two mixing products belonging to different subsets are uncoupled, the Jacobian matrix is reduced to a block-diagonal form, and the solution of the linear system required to compute the Newton update (7) is reduced to the solution of a number of uncoupled systems of smaller size, with a dramatic increase of numerical efficiency and an equally significant memory saving. From (11) and the first of (25) it is also evident that the parameter D represents the maximum difference between the orders of any two IM products that are considered coupled under the assumptions (25). It is thus possible to order the products belonging to each subset in such a way that the corresponding block subsystem be banded with a bandwidth depending on D. The best ordering criterion depends on the definition of the signal spectrum. This allows a band-matrix solver to be used for each block subsystem, with a further performance increase. If the first of (25) is suppressed, all the block subsystems are dense.

In many cases of practical interest, (25) do not only represent a mathematical assumption, but can be justified on a sound physical basis. Consider for instance an F-tone intermodulation problem, and assume for simplicity that the time delays in (3) are constant. If the input frequencies may be ordered in such a way that the last $F - H + 1$ are *very close* to each other in a relative sense, that is,

$$|\omega_i - \omega_j| \ll \omega_k \quad (H \le i, j \le F;\ 1 \le k \le F) \tag{26}$$

the IM products are clustered inside narrow frequency windows separated by large gaps. This kind of situation is very common in practice. In this case the spectrum may be conveniently described in terms of an auxiliary set of fundamentals defined by

$$\begin{aligned} \omega_i' &= \omega_i && (1 \le i \le H) \\ \omega_i' &= |\omega_i - \omega_H| && (H+1 \le i \le F). \end{aligned} \tag{27}$$

Due to (26), with the use of (27) each mixing product of the form (2) is a linear combination of H *high* and $F - H$ *low* frequencies. If we now consider a generic waveform (1) as a function defined on a multidimensional time space $[\omega_1' t, \omega_2' t, \omega_3' t, \cdots]$, then under (27) the last $F - H$ time variables are *slowly changing* with respect to the first H ones. In such conditions the second of (25) takes the meaning of a quasi-stationary approximation. This means that the slow dependence on time of the derivatives (10) through $\omega_i' t$ ($i \ge H + 1$) is considered negligible in comparison with the fast dependence through $\omega_1 t, \cdots \omega_H t$ in the time window (sufficiently longer than $2\pi/\omega_1$) used to compute the FFT. From this approximation, the second of (25) follows immediately. A similar conclusion can be reached when the last $F - H$ of the exciting frequencies are naturally small with respect to the first H ones, as it is the case in most modulation problems. In all such situations the decoupling of the equations occurs almost naturally, so that the Newton iteration based on the block-diagonal Jacobian is usually very robust. The first of (25) has simply the meaning of a possible truncation criterion for the multiple Fourier expansion of the derivatives. In any case the approximation is applied to the derivatives only, so that the solution of (6) is exact, provided that convergence be achieved.

In some situations, a structurally similar decoupling of the Jacobian into diagonal blocks can also be arrived at by the recently proposed [28] "frequency-windowing harmonic-balance" (FWHB) technique. The time-domain quasi-stationary approximation leading to the second of (25) is in a sense the dual of the assumption of constant linear-subnetwork admittance in each frequency window made by the FWHB [28], which is equivalent to considering $\boldsymbol{Y}(\omega)$ a slowly changing function of the "small" ω_i'. Of course, (25) only represents one possible application of the general MFFT-based sparse-matrix technique discussed in this section.

The application of the sparse-matrix technique to the above-mentioned mixer intermodulation problem is illustrated in Fig. 5. For this case we choose $H = 1$ in (25), and partition the spectrum defined by (24) into one-dimensional subsets of size $(2N_O + 1) \times (2N_O + 1)$ in terms of submatrices of the form (8). Each subset is characterized by constant values of $|k_2|$, $|k_3|$. Furthermore, if we choose $D = 3$ in (25) and order the IM products in each subset for increasing values of k_1, we obtain the sparsity pattern depicted in Fig. 5, where shaded and blank rectangles are representative of nonzero and zero submatrices, respectively. As expected, the Jacobian is reduced to a block-diagonal structure, and each uncoupled subsystem is banded (with bandwidth D in this special case). In this way, the memory occupation of the Jacobian drops to about 8 MB, which is compatible with the memory resources of most typical engineering workstations. Also, the cost of one Newton iteration is reduced by a factor of about 300 with respect to the dense-Jacobian case on a SUN SPARCstation 2 in double-precision arithmetics. The tradeoff with power-handling capabilities is excellent for ordinary applications. With the sparsity pattern depicted in Fig. 5 the circuit can be analyzed

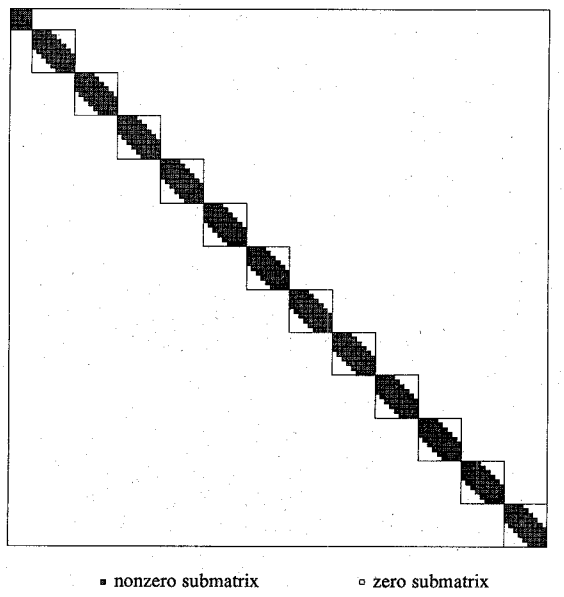

Fig. 5. Pattern of nonzero submatrices of the Jacobian for a 2-tone intermodulation analysis of the distributed mixer ($H = 1$, $D = 3$).

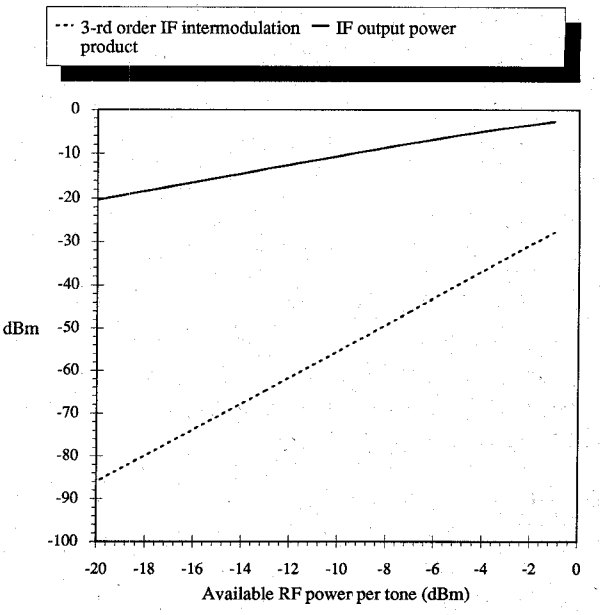

Fig. 6. Fundamental IF output at $\omega_2 - \omega_1$, and 3rd order IF intermodulation product at $2\omega_3 - \omega_2 - \omega_1$ for the distributed mixer under 2-tone RF excitation.

without convergence problems well beyond the LO power level for which conversion gain is a maximum at low RF power levels, and well beyond the 1 dB compression point in maximum-gain conditions.

Fig. 6 shows the computed results of the mixer intermodulation distortion analysis with $\omega_1/2\pi = 3$ GHz, $\omega_2/2\pi = 3.51$ GHz, $\omega_3/2\pi = 3.511$ GHz. The (equal) power levels of the two RF tones are swept from -20 to -1 dBm in 1 dB steps, with the upper bound now corresponding to a gain compression of about 1.3 dB because of the two-tone RF excitation (see section II). The accuracy of the results was checked and found excellent by a Cray analysis run with 8 LO harmonics and intermodulation products up to the 5th order [25]. The average analysis cost on the SUN SPARCstation 2 workstation is about 120 s per point. The same approach can be successfully applied even to simulation problems of smaller numerical size. As an example, a regular analysis of the same mixer under the same conditions described in Section II (432 scalar unknowns) may be carried out with a derivatives spectrum defined by (25) with $H = 1$, $D = 1$. The single low-level analysis ($P_{LO} = +13$ dBm, $P_{RF} = -20$ dBm) takes about 25 CPU s on the SUN 2, and thus becomes cost-competitive with the frequency-conversion analysis. In addition, the mixer dynamic range can be determined in this way without any convergence problems.

An important limiting case of the sparse-matrix approach is obtained when the derivatives spectrum contains the dc component only ($D = 0$ in (25)). This leads to the so-called block-Newton iteration [29], whereby only couplings between identical frequency components are taken into account. Since this is a rather drastic approximation, this kind of analysis has limited power-handling capabilities, and is often insufficient to establish the dynamic range of typical nonlinear circuits. Nevertheless, this approach is very useful for the fast computation of some important small-signal nonlinear quantities such as the 3rd and 5th order intercept points. With the block-Newton iteration, both the memory occupation and the factorization time of the Jacobian become negligible, and the harmonic-balance analysis may become cost-competitive with small-signal techniques such as Volterra series or the related method of nonlinear currents [30], [31].

As a typical example, let us consider once again a three-tone intermodulation analysis of the distributed amplifier shown in Fig. 3 (6 device ports and 77 circuit nodes). At low input power levels, say -10 dBm per tone, the computation of near-carrier intermodulation products up to the 5th order by the block-Newton iteration coupled with the multiple fast Fourier transform algorithm takes about 25 s on a SUN SPARCstation 2. What is more important, the nonlinear aspects give only a minor contribution, of the order of 24 percent, to the overall analysis cost, which is dominated by the linear subnetwork analysis. It is thus clear that the use of a different frequency-domain nonlinear analysis approach could only result in a minor improvement of the simulation speed. Thus, although the method of nonlinear currents (e.g., in the implementation proposed by Maas [32]) is probably the fastest way of carrying out a low-level multitone analysis, the block-Newton HB technique in this and other similar cases can reach a comparable efficiency. However, in the present case convergence can be obtained only up to a gain compression level of about 0.4 dB even making use of all the methods for convergence improvement discussed in Section III.

As it may be easily inferred from the numerical performance information reported above, the sparse-matrix approach described in this section can literally outperform other more conventional harmonic-balance algorithms,

including some commercial ones, with speedup factors that may range up to two orders of magnitude or more for relatively complex circuit topologies. It thus opens the way to a number of advanced applications of the HB technique that would be hardly feasible by standard methods, such as the frequency-domain transient simulations discussed in Section V.

V. Pulsed-RF and Transient Analysis

The simulation of nonlinear microwave circuits operated under pulsed RF conditions is an intriguing problem from the CAD viewpoint. In principle one could obviously resort to time-domain simulators [33], which can handle any signal waveform without restriction. However, the well-known limitations of time-domain techniques in the treatment of passive circuits virtually restrict this kind of approach to simple topologies only containing lumped elements and elementary types of distributed components. On the contrary, many practical microwave circuits contain passive integrated components which can only be characterized in the frequency domain by electromagnetic methods, especially at high frequencies [34]. For these cases a nonlinear analysis in pulsed RF conditions is still an open problem.

When the pulses form a periodic sequence, a pulsed RF regime is a special form of steady-state regime. It is thus intuitive that numerical techniques explicitly aimed at steady-state analysis, such as harmonic balance, should represent a possible way to do the job. The purpose of this section is to show that this kind of analysis is, indeed, feasible making use of a harmonic-balance simulator incorporating the previously described capabilities. An interesting point is that, for pulse durations long enough with respect to the RF period, the analysis approach presented in this section also provides a direct way of performing a transient analysis by harmonic-balance methods. It has been found that in the case of lumped-element topologies that can be treated in the time domain, the results of our HB technique are consistent with those provided by classic time-domain simulators such as SPICE.

Let us consider a nonlinear circuit excited by an RF sinusoidal source of angular frequency ω_1 (*carrier*) modulated by a periodic signal $s(t)$ of period $2\pi/\omega_2$. For the applications of interest in this section, $s(t)$ is ideally a sequence of rectangular pulses, which for practical purposes is approximated by a truncated Fourier expansion. Thus we have

$$s(t) = \sum_{k_2=-N}^{N} S_{k_2} \exp(jk_2\omega_2 t) \tag{28}$$

where $S_{-k_2} = S_{k_2}^*$. In practice, a non-ideal pulse waveform with finite rise and fall times [35] is used in order to keep these quantities under control. As an example, in Fig. 7 the sum of (28) with $N = 50$ is plotted against time for a sequence of rectangular pulses having a duty cycle of 30% and rise and fall times equal to 5% of the pulse repetition time.

In agreement with (1), the unmodulated input signal is represented by

$$v(t) = 2 \operatorname{Re}[V_1 \exp(j\omega_1 t)] \tag{29}$$

so that the modulated excitation becomes

$$u(t) = v(t)\, s(t) = 2 \operatorname{Re}\left\{ \sum_{k_2=-N}^{N} V_1 S_{k_2} \exp[j(\omega_1 + k_2\omega_2)t] \right\}. \tag{30}$$

From a conceptual viewpoint, we can think of (30) as being the output of an ideal amplitude modulator whose two inputs are fed by (28) and (29). Thus a generic nonlinear circuit excited by (30) can be replaced by an augmented circuit (obtained by connecting the ideal modulator to the input port of the original one) excited by two periodic sources of frequencies ω_1, ω_2. In general, the analysis of a nonlinear circuit under pulsed RF conditions can thus be treated as a two-tone IM analysis problem. In the mixer case, an RF signal of the form (30) is superimposed on the local-oscillator regime, so that by a similar argument the analysis can be reduced to a three-tone IM problem.

In the two-tone case, a suitable definition of the signal spectrum is [36]

$$\boldsymbol{S} \triangleq \begin{cases} 0 \le |k_1| \le M \\ 0 \le |k_2| \le N \end{cases} \tag{31}$$

where M is the number of carrier harmonics to be considered in the CW analysis of the same circuit. For mixer analysis a spectrum similar to (31) is repeated on each side of every local-oscillator harmonic of interest.

For computational purposes, our harmonic-balance simulator was modified to accept modulated sources besides conventional CW sources as standard excitations. The Fourier coefficients of the modulating signal are computed once for all and are stored in the computer memory. The RF source is simply defined by means of the complex amplitude $2V_1$ and of the indication that the source is modulated. Then, according to (28), the program automatically connects in series to the RF input port $2N + 1$ sinusoidal sources of complex amplitudes $2V_1S_{k_2}$ and frequencies $\omega_1 + k_2\omega_2$ ($0 \le |k_2| \le N$). At this stage the multitone harmonic-balance analysis can proceed in the way discussed in Section II. It is noteworthy that the program also allows the modulation defined by (28) to be applied to the bias sources. The two cases do not differ conceptually nor computationally, and in particular the intermodulation spectrum may always be defined by (31). In this case the program connects in series to the bias port of interest a dc source E_0S_0 and N sinusoidal sources of complex amplitudes $2E_0S_{k_2}$ at frequencies $k_2\omega_2$ ($1 \le k_2 \le N$), where E_0 is the unmodulated bias voltage. The pulsed bias can also be offset in order to include circuits periodically switched between two different bias levels.

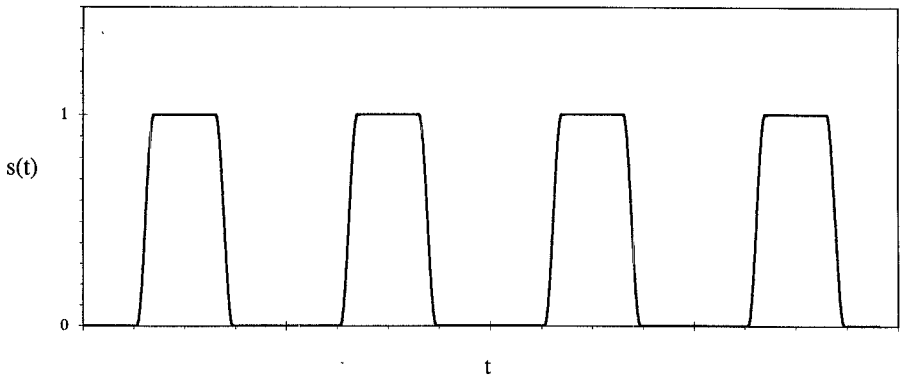

Fig. 7. Approximation of a periodic sequence of rectangular pulses having 5% rise and fall times and 30% duty cycle (50 harmonics).

This facility is intended to allow the simulation of a number of interesting events such as turnon transients in amplifiers and oscillators, and tuning transients in VCO's. Further work on these subjects will be reported elsewhere.

The pulsed-RF analysis outlined in this section is a rather ill-conditioned job from the numerical viewpoint. The main numerical difficulties arise from the following aspects.

1) The problem is strongly nonlinear because of the simultaneous occurrence of heavily driven devices (such as saturated FET's, or BJT's in class-C operation) and multitone excitation.

2) The number of spectral components to be balanced is usually large. Relatively large values of N are required to minimize the unwanted ripples produced by the truncation of the series (28), and several carrier harmonics must be considered for circuits operating in saturation. The use of several hundreds of frequencies is thus customary even for simple circuit topologies, and this often leads to nonlinear solving systems with thousands of scalar unknowns.

As a consequence, the advanced features described in the previous sections usually represent a prerequisite for the HB simulator to be able to carry out successfully this kind of analysis with practically acceptable efficiency. In particular, the mechanisms described in Section III for enhancing the robustness of the iteration, and the sparse-matrix techniques introduced in Section IV are of primary importance. This will be illustrated by a typical example.

Let us consider a microstrip amplifier having the topology schematically illustrated in Fig. 8. The FET is a 600 μm device described by a modified Materka and Kacprzak model [37], and radial microstrip stubs are used both in the RF matching sections and in the bias circuit. The amplifier has a saturated power output (at the 4 dB gain-compression level) of +25.3 dBm with 6 dB of associated gain across a 2 GHz band centered around 10 GHz. The input signal is a 10 GHz sinusoid modulated by a periodic sequence of rectangular pulses having a pulse repetition frequency of 10 MHz, rise and fall times of 5 ns, and a duty cycle of 30% (see Fig. 7). The analysis is carried out with the spectrum defined by (31) with $M = 4$ and N

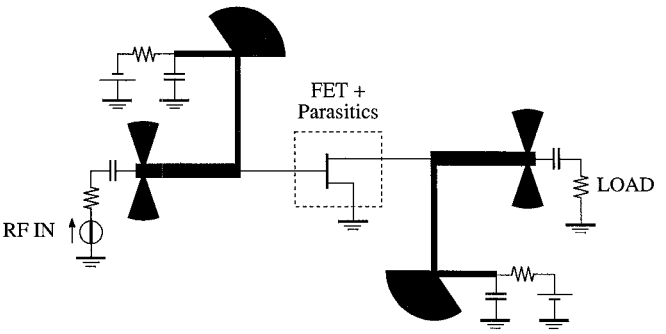

Fig. 8. Schematic topology of a microstrip power amplifier using radial stubs.

$= 50$, for a total of $n_H = 909$ spectral lines. This corresponds to 1818 scalar unknowns, and to a memory occupation of 26.5 MB for the full Jacobian.

In spite of the simple circuit topology, this problem is difficult to handle on a workstation with 16 MB of physical memory, because the data transfers to and from the virtual memory make the Jacobian factorization process very inefficient. Thus, for a general-purpose implementatin of the pulsed-RF analysis approach, the use of the sparse-matrix technique discussed in Section IV is virtually mandatory. The excellent results obtained by this method making use of the derivatives spectrum (25) are shown in Fig. 9. In this figure the analysis time on the SUN 2 is plotted against the peak input power, for $H = 1$ and $D = 4$. With this choice the structure of the sparse Jacobian is similar to the one shown in Fig. 5. The only differences are that the number of uncoupled subsystems is now equal to 51, and that each block subsystem has a bandwidth of 4 in terms of nonzero submatrices. The memory occupation of the Jacobian is only 0.52 MB. The peak input power levels considered in Fig. 9 range from +10.3 dBm, which is well inside the linear region (approximately 0.1 dB gain compression), up to +25.3 dBm, which is far into the saturation region (0 dB gain level, corresponding to 10 dB compression). In all cases the analysis is started from zero harmonics (no starting-point information). It is noteworthy that the CPU time required for a pulsed-RF analysis is less than 180 s at the 4 dB compression level. These results confirm the statement

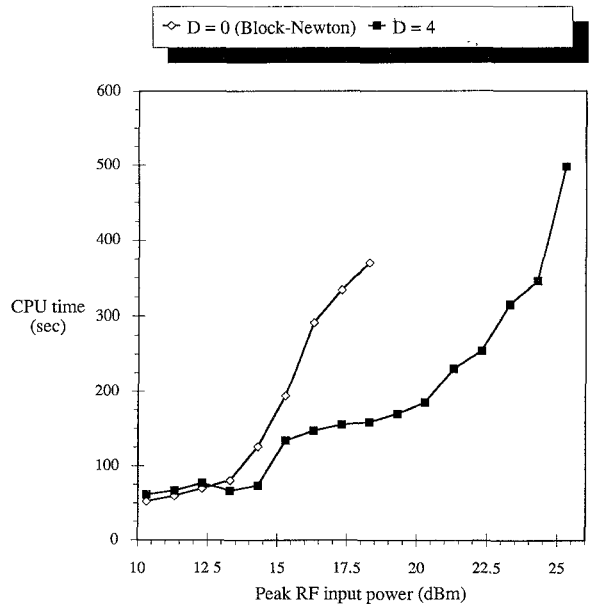

Fig. 9. Performance of a sparse-matrix analysis of the power amplifier under pulsed-RF excitation.

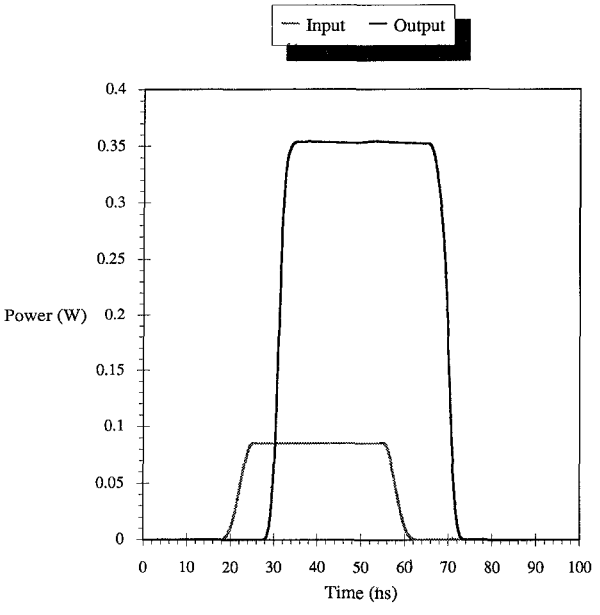

Fig. 10. Power envelopes of the input and output RF pulses for the power amplifier with a 3-m long transmission line connected to the output port.

made in Section IV, that the analysis based on the block-diagonal Jacobian is usually very robust. The choice $D = 4$ was empirically found to represent an optimum. For $D > 4$, no significant improvement of the power-handling capabilities of the analysis algorithm is observed. On the other hand, for $D < 4$ the analysis slows down considerably at high power levels, while the speed advantage at low power levels is negligible. For comparison, the curve obtained for $D = 0$ (corresponding to a block-Newton iteration) is also reported in Fig. 9. In this case the algorithm is unable to converge at the nominal input level of +19.3 dBm.

Fig. 10 shows the power envelopes [36] of the input and output signals at the nominal peak input power level of +19.3 dBm (4 dB compression). The group delay of the amplifier is about 0.43 ns, which cannot be appreciated with the time scale used in Fig. 10. Thus, in order to show the excellent phase control provided by the numerical analysis, an ideal transmission line 3m long was added between the output port and the load. The result, as expected, is a 10 ns delay of the output pulse, which is clearly evident in Fig. 10.

Note that it would be virtually impossible to carry out the same transient analysis by time-domain techniques, because of the radial microstrip stubs for which an accurate characterization is only available in the frequency domain [34].

VI. Broadband Optimization

In a sense, a nonlinear circuit is always a broadband circuit because the spectrum of the steady-state waveforms always includes several discrete lines and thus covers a finite bandwidth. In this section, however, we shall define as *broadband* [1] a circuit whose performance is simultaneously specified for a number of independent steady-state regimes having different spectra. Such spectra are usually (but not necessarily) obtained from one another by changing the frequencies of one or more of the exciting sinusoidal signals. Thus for nonlinear circuit optimization the concept of *design spectra* represents the natural extension of the familiar concept of design frequencies encountered in linear circuit design. In turn, an independent state vector is associated with each spectrum, so that the set of problem unknowns includes all these state vectors and the set $\boldsymbol{P}$ of optimizable parameters. The latter may include linear and nonlinear subnetwork parameters as well as the impressed voltages of any of the free sources. In this section we discuss the implementation of an efficient broadband optimization capability in our general-purpose harmonic-balance simulator [1].

The electrical performance of a nonlinear circuit may be described in terms of a set of network functions which are dependent both on the electrical regime (i.e., the state vector $\boldsymbol{X}$) and on the optimizable parameters. A generic network function is thus denoted by $F^{(i)}(\boldsymbol{X}, \boldsymbol{P})$, and a generic design goal is stated in the form

$$F^{(i)}_{\min} \leq F^{(i)}(\boldsymbol{X}, \boldsymbol{P}) \tag{32}$$

where the index i spans all the specifications and all the design spectra. From a mathematical viewpoint, the optimization process can be viewed as the search for a set $\boldsymbol{P}$ of variables for which the design goals are satisfied in the best possible way, subject to the constraint that the state lies on the manifold $\boldsymbol{M} \equiv [\boldsymbol{X} = \boldsymbol{X}(\boldsymbol{P})]$ implicitly defined by (6). In order to fulfill this constraint, prior to each objective function evaluation the circuit defined by the current value of $\boldsymbol{P}$ is analyzed at each design spectrum by the Newton-iteration based HB technique. The network functions are then computed at each spectrum by a conventional analysis of the linear subnetwork operating in the

electrical regime defined by $\boldsymbol{X}(\boldsymbol{P})$. Thus for each design goal the specification (32) may be associated with the error function

$$E^{(i)}(\boldsymbol{P}) = w^{(i)} \cdot [F^{(i)}_{\min} - F^{(i)}(\boldsymbol{X}(\boldsymbol{P}), \boldsymbol{P})] \tag{33}$$

where $w^{(i)}$ is a positive weight. A suitable choice for an objective encompassing all the design goals is the generalized ℓ_p function [38]

$$F_{OB}(\boldsymbol{P}) = \begin{cases} \left\{ \sum_i^{+} [E^{(i)}(\boldsymbol{P})]^p \right\}^{1/p} & \text{if } E_{\max} \geq 0 \\ -\left\{ \sum_i [-E^{(i)}(\boldsymbol{P})]^{-p} \right\}^{-1/p} & \text{if } E_{\max} < 0 \end{cases} \tag{34}$$

where $E_{\max}$ is the maximum error (in the algebraic sense), and the superscript $^+$ indicates that the summation is extended to positive errors only. For $p > 1$ the objective is differentiable, and can be minimized with respect to $\boldsymbol{P}$ by an efficient gradient-based minimizatin algorithm [39]. The program makes use of the quasi-Newton method discussed in [40].

As in the analysis case, the use of an exact formula for the computation of the gradients is essential in order to achieve the best performance of the optimization algorithm [1], [41]. By means of (33) and (34), the derivative of the objective with respect to a generic optimizable parameter P is directly related to the derivatives of the network functions $F^{(i)}$ wrt. the same quantity. Any such derivative will be denoted by the symbol D when it is taken on the manifold $\boldsymbol{M}$. We have

$$\frac{DF^{(i)}}{DP} = \left.\frac{\partial F^{(i)}}{\partial P}\right|_{X=\text{const}} + \left.\left(\frac{\partial F^{(i)}}{\partial \boldsymbol{X}}\right)^T\right|_{P=\text{const}} \cdot \frac{D\boldsymbol{X}}{DP} \tag{35}$$

In principle, exact methods are available for the computation of all terms in (35). First of all, differentiating (6) yields

$$\frac{D\boldsymbol{X}}{DP} = -[\boldsymbol{J}(\boldsymbol{X})]^{-1} \cdot \left.\frac{\partial \boldsymbol{E}}{\partial P}\right|_{X=\text{const}} \tag{36}$$

where $\boldsymbol{J}$ is the Jacobian matrix of $\boldsymbol{E}$ with respect to $\boldsymbol{X}$, as in Section II. From (5) we get

$$\left.\frac{\partial \boldsymbol{E}_k}{\partial P}\right|_{X=\text{const}} = \frac{\partial \boldsymbol{Y}}{\partial P}(\Omega_k)\, \boldsymbol{U}_k(\boldsymbol{X}) + \frac{\partial \boldsymbol{N}}{\partial P}(\Omega_k) \tag{37}$$

$$\left.\frac{\partial \boldsymbol{E}_k}{\partial P}\right|_{X=\text{const}} = \frac{\partial \boldsymbol{N}}{\partial P}(\Omega_k) \tag{38}$$

$$\left.\frac{\partial \boldsymbol{E}_k}{\partial P}\right|_{X=\text{const}} = \boldsymbol{Y}(\Omega_k) \frac{\partial \boldsymbol{U}_k}{\partial P} + \frac{\partial \boldsymbol{W}_k}{\partial P} \tag{39}$$

where (37) has to be used for a linear subnetwork parameter, (38) for a source voltage, and (39) for a nonlinear subnetwork parameter. The derivatives appearing on the right-hand side of (39) can be evaluated as the Fourier coefficients of $\partial \boldsymbol{u}/\partial P$, $\partial \boldsymbol{w}/\partial P$.

Since the network functions are obtained from a linear subnetwork analysis, they are expressed in terms of the voltage harmonics at the device ports, of the source voltages, and of the admittance parameters y_{ij} of an "augmented" linear subnetwork [42]. The latter is obtained by cutting the load and source branches, and thus creating as many additional ports. Thus a generic subvector of $\partial F^{(i)}/\partial \boldsymbol{X}|_{P=\text{const}}$ takes the form

$$\left.\frac{\partial F^{(i)}}{\partial \text{ Re } [\boldsymbol{X}_s]}\right|_{P=\text{const}} = \sum_{k \in S} \left\{ \frac{\partial F^{(i)}}{\partial \text{ Re } [\boldsymbol{U}_k]} \frac{\partial \text{ Re } [\boldsymbol{U}_k]}{\partial \text{ Re } [\boldsymbol{X}_s]} + \frac{\partial F^{(i)}}{\partial \text{ Im } [\boldsymbol{U}_k]} \frac{\partial \text{ Im } [\boldsymbol{U}_k]}{\partial \text{ Re } [\boldsymbol{X}_s]} \right\} \tag{40}$$

A similar equation holds for the derivative with respect to Im $[\boldsymbol{X}_s]$. In (40) the derivatives of $F^{(i)}$ wrt. the voltage harmonics at the device ports may be obtained explicitly from the augmented linear subnetwork analysis. In turn, the exact derivatives of the voltage harmonics wrt. the state-variable harmonics are evaluated by (11), (12).

Finally, we may write

$$\left.\frac{\partial F^{(i)}}{\partial P}\right|_{X=\text{const}} = \sum_{k \in S} \left\{ \sum_{i,j} \left[\frac{\partial F^{(i)}}{\partial y_{ij}(\Omega_k)} \frac{\partial y_{ij}(\Omega_k)}{\partial P} \right] + \left(\frac{\partial F^{(i)}}{\partial \boldsymbol{N}(\Omega_k)} \right)^T \frac{\partial \boldsymbol{N}}{\partial P}(\Omega_k) \right\} \tag{41}$$

$$\left.\frac{\partial F^{(i)}}{\partial P}\right|_{X=\text{const}} = \sum_{k \in S} \left\{ \left(\frac{\partial F^{(i)}}{\partial \boldsymbol{N}(\Omega_k)} \right)^T \frac{\partial \boldsymbol{N}}{\partial P}(\Omega_k) \right\} \tag{42}$$

$$\left.\frac{\partial F^{(i)}}{\partial P}\right|_{X=\text{const}} = \sum_{k \in S} \left\{ \frac{\partial F^{(i)}}{\partial \text{ Re } [\boldsymbol{U}_k]} \frac{\partial \text{ Re } [\boldsymbol{U}_k]}{\partial P} + \frac{\partial F^{(i)}}{\partial \text{ Im } [\boldsymbol{U}_k]} \frac{\partial \text{ Im } [\boldsymbol{U}_k]}{\partial P} \right\} \tag{43}$$

where (41) has to be used for a linear subnetwork parameter, (42) for a source voltage, and (43) for a nonlinear subnetwork parameter. Once again, the derivatives of $F^{(i)}$ with respect to y_{ij} and $\boldsymbol{N}$ may be obtained explicitly from the augmented linear subnetwork analysis. If P is a linear subnetwork parameter, the derivatives of the admittance parameters with respect to P may be found (at least in principle) by adjoint-network calculations [43]. Note that in practice very few terms of the summations appearing in (40)–(43) are nonzero for a typical network function.

Finally, it should be observed that in practice some of the terms of the above derivatives may be more conveniently computed by numerical perturbations, without impairing the accuracy of the gradient evaluation procedure. A typical example is given by $\partial y_{ij}/\partial P$ when the linear

subnetwork admittance matrix is computed numerically by electromagnetic methods.

An essential point is that a factorization of the Jacobian is automatically known at each design spectrum from the Newton iteration performed to analyze the nonlinear circuit for the current set of parameters $\boldsymbol{P}$, and does not require any additional computation. Thus the Newton iteration represents the best choice for a harmonic-balance algorithm to be coupled with an optimization process, since it makes automatically available the key information required for the exact computation of the gradients. This property is not shared by any other of the iteration schemes that are commonly in use for solving the harmonic-balance equations. It is worth noting that another nonlinear analysis technique that has been effectively coupled with optimization, is the method of nonlinear currents [44], with the usual restriction to weakly nonlinear situations. The tradeoff here is between CPU time and generality of application. With the harmonic-balance approach described in this section, microwave circuits can be optimized at any drive level. As an example, the program can compute at run time and directly optimize the gain compression of an amplifier. This allows a power amplifier to be optimized at a prescribed compression level, e.g., in order to find the best compromise among output power, efficiency, and transducer gain over a frequency band.

Fig. 11 shows the circuit topology of a single-ended FET gate mixer which will be used to monitor the performance of the broadband optimization algorithm in a typical application. The circuit simply consists of a common-source FET with a low-pass filter on the drain and a two-section reactive matching network connected with the gate. Both the RF and the LO signals are injected into the gate. The FET is a small-signal device corresponding to an Avantek 8251 with an I_{DSS} of 80 mA, once again described by a modified Materka and Kacprzak model [37].

Fig. 12 shows the transducer conversion gain of the mixer as a function of the IF frequency when a standard Butterworth design is chosen for the IF filter, and arbitrary values of 1 nH and 1 pF are assigned to the inductances and capacitances of the input matching network. Starting from this point the circuit is optimized for a minimum conversion gain of 7.5 dB and a minimum input return loss of 15 dB across an IF band ranging from 0.1 to 1.3 GHz. Performance specifications are assigned at 7 different IF values with a constant LO frequency of 8 GHz. The optimization variables are the inductances and capacitances of the input matching network plus the gate bias voltage, which is known to have a major influence on the mixer performance.

The results obtained after 8 iterations are again given in Fig. 12 for the transducer conversion gain, and in Fig. 13 for the RF input return loss. The nice equal-ripple behavior of the optimized performance and the small number of iterations are clear checks of the excellent numerical behavior of the optimization algorithm. As a matter of fact, the algorithmic efficiency of this design procedure

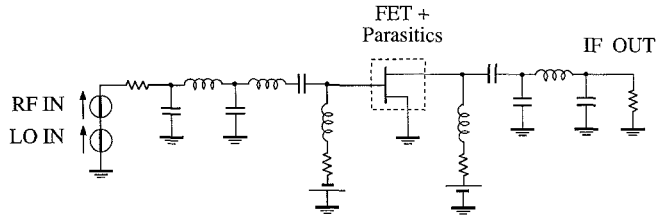

Fig. 11. Schematic topology of a broadband FET gate mixer.

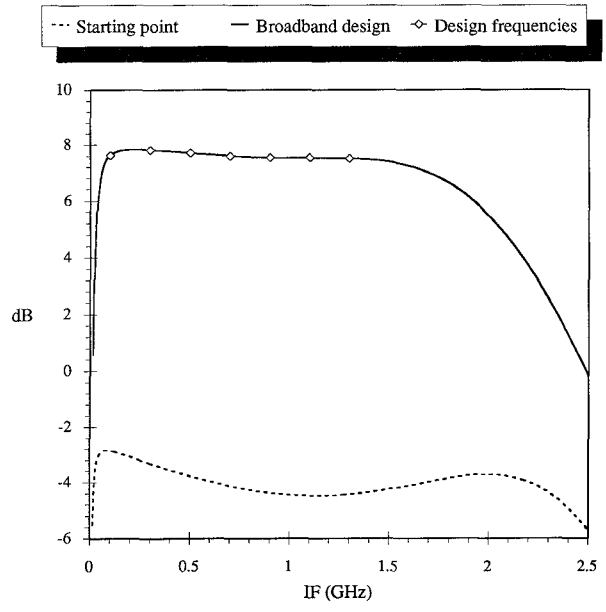

Fig. 12. Starting-point and optimized transducer conversion gain of the broadband mixer.

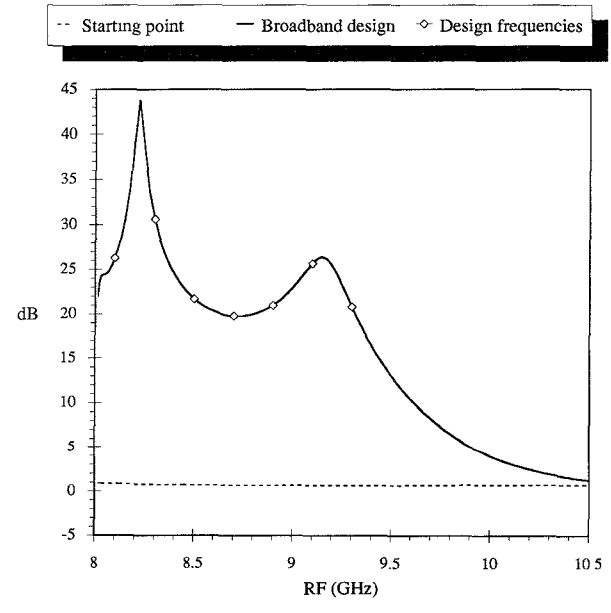

Fig. 13. Starting-point and optimized RF input return loss of the broadband mixer.

for nonlinear circuits is very close to the performance we are familiar with in linear circuit design, in the sense that the required number of iterations for a given set of design frequencies and a given number of optimization variables

is pretty much the same in the two cases. In other words, the ratio between a nonlinear and a linear design cost is very close to the ratio between a nonlinear and a linear analysis cost of the same circuit topology. The overall CPU time required by this optimization is about 130 s on a SUN SPARCstation 2. Similar results were obtained for other typical nonlinear subsystems [1]. It is thus clear that the numerical efficiency of the broadband optimization algorithm is high enough to warrant a systematic use of this technique at the workstation level.

REFERENCES

[1] V. Rizzoli, A. Costanzo, and C. Cecchetti, "Numerical optimization of broadband nonlinear microwave circuits," in *1990 IEEE MTT-S Int. Microwave Symp. Dig.*, Dallas, May 1990, pp. 335–338.

[2] J. W. Bandler, Q. J. Zhang, J. Song, and R. M. Biernacki, "Yield optimization of nonlinear circuits with statistically characterized devices," in *1989 IEEE MTT-S Int. Microwave Symp. Dig.*, Long Beach, CA, June 1989, pp. 649–652.

[3] J. Fitzpatrick and T. Cutler, "From CAE to measurements and documentation—one program in the 90's," *Applied Microwave Magazine*, pp. 88–96, May 1989.

[4] M. S. Nakhla and J. Vlach, "A piecewise harmonic-balance technique for determination of periodic response of nonlinear systems," *IEEE Trans. Circuits Syst.*, vol. CAS-23, pp. 85–91, Feb. 1976.

[5] K. S. Kundert and A. Sangiovanni-Vincentelli, "Simulation of nonlinear circuits in the frequency domain," *IEEE Trans. Computer-Aided Design*, vol. CAD-5, pp. 521–535, Oct. 1986.

[6] V. Rizzoli, C. Cecchetti, A. Lipparini, and F. Mastri, "General-purpose harmonic balance analysis of nonlinear microwave circuits under multitone excitation," *IEEE Trans. Microwave Theory Tech.*, vol. 36, pp. 1650–1660, Dec. 1988.

[7] W. R. Curtice, "Intrinsic GaAs MESFET equivalent circuit models generated from two-dimensional simulation," *IEEE Trans. Computer-Aided Design*, vol. 8, pp. 395–402, Apr. 1989.

[8] V. Rizzoli, C. Cecchetti, and A. Lipparini, "A general-purpose program for the analysis of nonlinear microwave circuits under multitone excitation by multidimensional Fourier transform," *Proc. 17th European Microwave Conf.*, Rome, Sept. 1987, pp. 635–640.

[9] E. Ngoya *et al.*, "Efficient algorithms for spectra calculations in nonlinear microwave circuits simulators," *IEEE Trans. Circuits Syst.*, vol. 37, pp. 1339–1355, Nov. 1990.

[10] R. J. Gilmore and M. B. Steer, "Nonlinear circuit analysis using the method of harmonic balance—a review of the art: Part II," *Int. J. Microwave Millimeter-Wave Computer-Aided Engineering*, vol. 1, no. 2, pp. 159–180, Apr. 1991.

[11] H. R. Yeager and R. W. Dutton, "Improvement in norm-reducing Newton methods for circuit simulation," *IEEE Trans. Computer-Aided Design*, vol. 8, pp. 538–546, May 1989.

[12] T. S. Howard and A. M. Pavio, "A distributed monolithic 2–18 GHz dual-gate MESFET mixer," in *IEEE 1987 Microwave and mm-Wave Monolithic Circuits Symp. Dig.*, Las Vegas, June 1987, pp. 27–30.

[13] V. Rizzoli and A. Neri, "State of the art and present trends in nonlinear microwave CAD techniques," *IEEE Trans. Microwave Theory Tech.*, vol. 36, pp. 343–365, Feb. 1988.

[14] D. A. Zein, "Solution of a set of nonlinear algebraic equations for general purpose CAD programs," in *Circuit Analysis, Simulation and Design*, A. E. Ruehli, Ed., New York: North Holland, 1986, pp. 207–279.

[15] H. Wacker, *Continuation Methods*. New York: Academic Press, 1978.

[16] V. Rizzoli and A. Neri, "Expanding the power-handling capabilities of harmonic-balance analysis by a parametric formulation of the MESFET model," *Electron. Lett.*, vol. 26, pp. 1359–1360, Aug. 1990.

[17] A. R. Kerr, "A technique for determining the local oscillator waveforms in a microwave mixer," *IEEE Trans. Microwave Theory Tech.*, vol. MTT-23, pp. 828–831, Oct. 1975.

[18] R. G. Hicks and P. J. Khan, "Numerical analysis of nonlinear solid-state device excitation in microwave circuits," *IEEE Trans. Microwave Theory Tech.*, vol. MTT-30, pp. 251–259, Mar. 1982.

[19] C. Camacho-Peñalosa, "Numerical steady-state analysis of nonlinear microwave circuits with periodic excitation," *IEEE Trans. Microwave Theory Tech.*, vol. MTT-31, pp 724–730, Sept. 1983.

[20] B. Schüppert, "A fast and reliable method for computer analysis of microwave mixers," *IEEE Trans. Microwave Theory Tech.*, vol. MTT-34, pp. 110–119, Jan. 1986.

[21] V. Rizzoli, F. Mastri, and C. Cecchetti, "A highly efficient p-n junction model for use in harmonic-balance simulation," in *Proc. 19th European Microwave Conf.*, London, Sept. 1989, pp. 979–984.

[22] J. H. Haywood and Y. L. Chow, "Intermodulation distortion analysis using a frequency-domain harmonic balance technique," *IEEE Trans. Microwave Theory Tech.*, vol. 36, pp. 1251–1257, Aug. 1988.

[23] V. Rizzoli, C. Cecchetti, and A. Costanzo, "Computer-aided design of class-C microwave transistor amplifiers by direct numerical optimization," in *1989 IEEE MTT-S Int. Microwave Symp. Digest.*, Long Beach, CA, June 1989, pp. 585–588.

[24] S. A. Maas, "Two-tone intermodulation in diode mixers," in *IEEE Trans. Microwave Theory Tech.*, vol. MTT-35, pp. 307–314, Mar. 1987.

[25] V. Rizzoli *et al.*, "Modern perspectives in supercomputer-aided microwave circuit design," *Int. J. Microwave Millimeter-Wave Computer-Aided Engineering*, vol. 1, no. 2, pp. 201–224, Apr. 1991.

[26] V. Rizzoli, F. Mastri, F. Sgallari, and V. Frontini, "The exploitation of sparse-matrix techniques in conjunction with the piecewise harmonic-balance method for nonlinear microwave circuit analysis," in *1990 IEEE MTT-S Int. Microwave Symp. Dig.*, Dallas, pp. 1295–1298, May 1990.

[27] V. Rizzoli *et al.*, "Intermodulation analysis of microwave mixers by a sparse-matrix method coupled with the piecewise harmonic-balance technique," in *Proc. 20th European Microwave Conf.*, Budapest, Sept. 1990, pp. 189–194

[28] F. Filicori, V. A. Monaco, and G. Vannini, "Computationally efficient intermodulation analysis of GaAs MESFET amplifiers and mixers," in *Proc. 3rd International Workshop on GaAs in Telecommunications*, Vimercate, Mar. 1991, pp. 117–129.

[29] C.-R. Chang, P. L. Heron, and M. B. Steer, "Harmonic balance and frequency-domain simulation of nonlinear microwave circuits using the block Newton method," *IEEE Trans. Microwave Theory Tech.*, vol. 38, pp. 431–434, Apr. 1990.

[30] J. J. Bussgang, L. Ehrman, and J. W. Graham, "Analysis of nonlinear systems with multiple inputs," in *Proc. IEEE*, vol. 62, pp. 1088–1119, Aug. 1974.

[31] S. A. Maas, *Nonlinear Microwave Circuits*. Norwood, MA: Artech House, 1988.

[32] ——, "A general-purpose computer program for the Volterra-series analysis of nonlinear microwave circuits," in *1988 IEEE MTT-S Int. Microwave Symp. Dig.*, New York, May 1988, pp. 311–314.

[33] M. I. Sobhy and A. K. Jastrzebski, "Computer-aided design of microwave integrated circuits," in *Proc. 14th European Microwave Conf.*, Liège, Sept. 1984, pp. 705–710.

[34] F. Giannini, R. Sorrentino, and J. Vrba, "Planar circuit analysis of microstrip radial stub," *IEEE Trans. Microwave Theory Tech.*, vol. MTT-33, pp. 129–135, Feb. 1985.

[35] E. D. Ostroff *et al.*, *Solid-State Radar Transmitters*. Norwood, MA: Artech House, 1985.

[36] V. Rizzoli *et al.*, "Pulsed-RF and transient analysis of nonlinear microwave circuits by harmonic-balance techniques," in *1991 IEEE MTT-S Int. Microwave Symp. Dig.*, Boston, June 1991, pp. 607–610.

[37] A. Materka and T. Kacprzak, "Computer calculation of large-signal GaAs FET amplifier characteristics," *IEEE Trans. Microwave Theory Tech.*, vol. MTT-33, pp. 129–135, Feb. 1985.

[38] C. Charalambous, "Nonlinear least pth optimization and nonlinear programming," *Mathematical Programming*, vol. 12, pp. 195–225, 1977.

[39] J. W. Bandler and S. H. Chen, "Circuit optimization: the state of the art," *IEEE Trans. Microwave Theory Tech.*, vol. 36, pp. 424–443, Feb. 1988.

[40] R. Fletcher, "A new approach to variable metric algorithms," *Computer J.*, vol. 13, pp. 317–322, Aug. 1970.

[41] J. W. Bandler, Q. J. Zhang, and R. M. Biernacki, "Practical, high speed gradient computation for harmonic balance simulators," in *1989 IEEE MTT-S Int. Microwave Symp. Dig.*, Long Beach, CA, June 1989, pp. 363–366.

[42] V. Rizzoli, A. Lipparini, and E. Marazzi, "A general-purpose program for nonlinear microwave circuit design," *IEEE Trans. Microwave Theory Tech.*, vol. MTT-31, Sept. 1983, pp. 762–770.

[43] K. C. Gupta, R. Garg, and R. Chadha, *Computer-Aided Design of Microwave Circuits*. Norwood, MA: Artech House, 1981.

[44] S. A. Maas, *C/NL: Linear and Nonlinear Microwave Circuit Analysis and Optimization Software and User's Manual*. Norwood, MA: Artech House, 1990.

Vittorio Rizzoli (M'79–SM'90) received the degrees in electronic engineering from the University of Bologna, Italy. His thesis dealt with the computer-aided analysis of multistrip components for MIC's, with particular emphasis on the design criteria for interdigitated couplers.

From 1971 to 1973 he held a research grant issued by Fondazione Ugo Bordoni, and joined the Centro Onde Millimetriche in Pontecchio Marconi, Bologna, where he was involved in the development of IF circuitry for a millimeter-wave circular-waveguide communications system. In 1973 he was with the Stanford Park Division of the Hewlett Packard Company, Palo Alto, CA, where he was engaged in microwave transistor modeling and medium-power amplifier design. In 1974 he joined the University of Bologna, Italy, as an Associate Professor of Circuit Theory, and in 1980 he became a Full Professor of Electromagnetic Fields and Circuits. His teaching and research activities have been devoted to several topics, including the theory of electromagnetic propagation in optical fibers, and the simulation and design of passive and active microwave integrated circuits. More recently, he has been engaged in the development of algorithms and software tools for the computer-aided design of nonlinear circuits, and among other, he has developed the first general-purpose harmonic-balance simulator with optimization capabilities. He has authored or co-authored over 80 technical papers in the fields of electromagnetic propagation, microwave circuit CAD, and related subjects.

Mr. Rizzoli is a member of the Technical Committee MTT-1 on Computer-Aided Design, the editorial board of the IEEE TRANSACTIONS ON MICROWAVE THEORY AND TECHNIQUES, and of John Wiley's *International Journal of Microwave and Millimeter-wave Computer Aided Engineering*. Since 1987, he has also been a member of the Technical Program Committee of the European Microwave Conference. In 1990–1991 he served as the Distinguished Microwave Lecturer of IEEE MTT-S for Region 8.

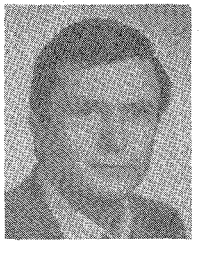

Alessandro Lipparini (M'88) was born in Bologna, Italy, on August 31, 1947. He graduated with a degree in electronic engineering from the University of Bologna, Bologna, Italy, in 1974.

In 1974, he joined the Technical Staff of the Istituto di Elettronica, University of Bologna, as a Research Fellow. Since March 1975, he has been a Researcher for the Italian Ministry of Education at the University of Bologna, also serving as a Lecturer on Circuit Theory and Electromagnetic Field Theory. In 1987 he joined the University of Bologna as an Associate Professor of Electromagnetic Fields and Circuits. Since then, he has been teaching a course on microwave integrated circuits. His current research interests are in the field of MIC and MMIC with special emphasis on nonlinear circuits. He is also involved in a research project aimed at the development of vectorized software for microwave circuit design applications.

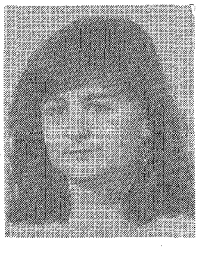

Alessandra Costanzo was born in Bologna, Italy, in May 1963. She graduated from the School of Electronic Engineering in July 1987.

In 1987 and 1988 she obtained a research grant issued by the Electronics Department of the University of Bologna and Telettra S.p.A., to carry out a study on carrier communications on power lines. In 1989 she joined the University of Bologna as a Researcher. Her research activity is currently devoted to nonlinear microwave and millimeterwave device modeling and characterization and to the development of software tools from microwave circuit optimization.

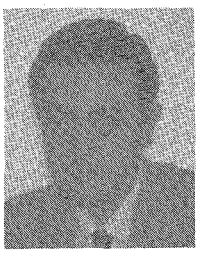

Franco Mastri was born in Forlì, Italy, in 1957. He received the degree in electronic engineering from the University of Bologna in 1985.

In 1987 and 1988 he obtained research grants issued by Fondazione Guglielmo Marconi, Pontecchio Marconi, Italy, and Selenia S.p.A., Rome, Italy to carry out a study on the application of nonlinear CAD techniques in MIC and MMIC design. In 1990 he joined the Istituto di Elettrotecnica of the University of Bologna as a Researcher. His research interests are in the field of nonlinear circuits, with particular emphasis on numeric methods for circuit simulation.

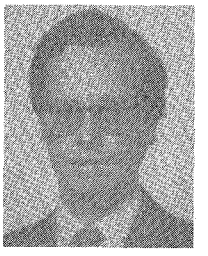

Claudio Cecchetti (M'89) was born in Forlì, Italy, in 1957. He received the degree in electronic engineering from the University of Bologna in October 1983.

In 1984–1985 he obtained a research grant issued by Fondazione G. Marconi, Pontecchio Marconi, Italy, to develop user-friendly interactive software for linear microwave circuits CAD. In 1985 he joined Fondazione U. Bordoni, Rome, Italy, where he is currently involved in research on nonlinear microwave circuits design. His main field of interest is the development of vectorized softwave for MIC and MMIC design applications.

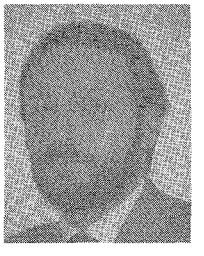

Andrea Neri (M'91) was born in Bologna in 1957. He received the degree in electronic engineering from the University of Bologna in 1981.

In 1983 and 1984 he obtained research grants issued by Fondazione G. Marconi, Pontecchio Marconi (Bologna), and Selenia S.p.A., Roma to work on dielectric resonators and their applications in MIC. In 1985 he joined Fondazione U. Bordoni, Roma, where he is currently involved in research on nonlinear microwave circuit design. In 1987 he received the Ph.D. degree in electronics and computer science. His main fields of interest are device modeling and the application of supercomputers in MIC and MMIC design.

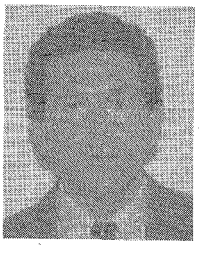

Diego Masotti was born in Bologna, Italy, in 1965. He received the electronic engineering degree from the University of Bologna in 1990. His thesis dealt with the computer-aided noise analysis of microwave mixers.

In January 1991 he obtained a research grant issued by Fondazione G. Marconi, Pontecchio Marconi, Italy, and Alenia S.p.a., Rome, Italy. His present research interests are in the area of microwave integrated circuit CAD, including the development of general-purpose software tools for the signal and noise simulation of nonlinear microwave subsystems.